Systematic Derivation of Dead-Zone Elimination Strategies for the Noninverting Synchronous Buck–Boost Converter

Neng Zhang, Guidong Zhang, *Member, IEEE*, and Khay Wai See

***Abstract*—The noninverting synchronous buck-boost converter is preferable to operate in buck and boost operating modes to obtain a high operating efficiency. However, the dead zone, which degrades the performance of the converter, will occur when the converter shifts from buck operating mode to boost operating mode or vice versa. Therefore, the origin of the dead zone is derived in this paper by analyzing the relationship between the voltage conversion ratio and the duty cycles of the switches. Based on this, a series of three-mode and four-mode modulation schemes are systematically derived to completely eliminate the dead zone. The ripple and average value of the inductor current under different modulation schemes are investigated to evaluate the performance of these modulation schemes. To demonstrate the effectiveness of the proposed modulation schemes, two implementations of a four-mode modulation scheme are presented and experimentally tested as the examples for all modulation schemes. Experimental results correspond well with the theoretical analysis in both implementations over the entire input voltage range.**

***Index Terms*—Dead-zone elimination strategies, noninverting synchronous buck–boost converter, smooth mode transition, systematic derivation.**

I. Introduction

THE noninverting synchronous buck–boost converter as shown in Fig. 1 can both boost and buck the input voltage to a noninverting output voltage. Also, voltage stresses of the power switches in this converter are lower than ones of other basic buck–boost converters, e.g., the inverting buck–boost converter, Cuk converter, Sepic converter, and Zeta converter [1], [2]. Therefore, the noninverting synchronous buck–boost converter has been investigated as a suitable candidate for those applications where the input voltage tends to vary in a wide range and overlap with the output voltage, such as power factor correction applications [3], [4] and fixed-configuration battery pack or reconfigurable battery pack based power systems [5], [6].

Manuscript received January 4, 2017; revised March 28, 2017; accepted May 6, 2017. Date of publication May 16, 2017; date of current version January 3, 2018. The work of N. Zhang was supported in part by the China Scholarship Council and in part by the University of Wollongong through Ph.D. scholarship. Recommended for publication by Associate Editor Ray-Lee Lin. *(Corresponding author: Khay Wai See.)*

N. Zhang and K. W. See are with the Institute for Superconducting & Electronic Materials, University of Wollongong, Wollongong, N.S.W. 2522, Australia (e-mail: nz970@uowmail.edu.au; kwsee@uow.edu.au).

G. Zhang is with the School of Automation, Guangdong University of Technology, Guangzhou 510006, China (e-mail: zgdscut@gmail.com).

Color versions of one or more of the figures in this paper are available online at http://ieeexplore.ieee.org.

Digital Object Identifier 10.1109/TPEL.2017.2704597

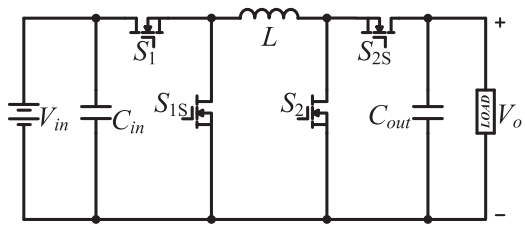

Fig. 1. Configuration of the noninverting buck–boost converter.

In order to operate with a high power conversion efficiency over the entire input voltage range, this converter is expected to operate in buck mode when the input voltage is higher than the output voltage and in boost mode when the input voltage is lower than the output voltage [7]–[14], which is called two-mode operating scheme in this paper. However, the converter will wigwag between the buck mode and the boost mode due to the practical unavoidable limitation of the electronic components when the input voltage is in a small range around the output voltage. Also, the discontinuity of the voltage conversion ratio will occur in this small range, which means that the voltage conversion ratio cannot reach the values around 1; therefore, this small range is called dead zone in this paper. The existence of the dead zone will lead to the increase of the output voltage ripple and potential instability of the converter [15]–[17].

Several solutions are developed to mitigate the dead-zone issue in the literature [5]–[20]. The simplest way is to control the converter solely operating in buck–boost mode at the cost of a decreased efficiency [19]. A complicated compensation method is proposed in [6] to avoid the dead zone. However, this method requires precise measurement of the details about the operating performance of the power devices, which is relatively difficult to execute in practical applications. A trimode two edge modulation method is proposed in [7]. In this modulation method, one duty cycle is clamped at the maximum value when the input voltage reaches the pre-assigned small range around the output voltage while the other duty cycle is controlled to regulate the output voltage. This method results in the fact that the limitation of the two duty cycles differs from each other and the lower limitation of the active duty cycle is required to be zero to completely eliminate the dead zone. However, the duty cycle can never reach zero due to the practical limitation of electronic components. A mix-mode modulation technique is proposed in [8] by inserting two additional buck–boost modes in the dead zone.

See http://www.ieee.org/publications_standards/publications/rights/index.html for more information.

This modulation method requires the switching frequency in the two additional buck–boost modes to be reduced by a half. A four-mode modulation scheme is proposed in [18]. The smooth mode transition can be obtained in this method by dividing the dead zone into two subzones and accordingly inserting two different buck–boost operating modes. By overlapping the duty cycles of both buck mode and boost mode and setting appropriate limitations of the duty cycles, an improved duty-cycle-overlap control method is proposed in [20]. With this control method, the pulse-skipping phenomenon can be well eliminated and smooth mode transition can be achieved. A comprehensive derivation of the dead zone avoiding methods is conducted in [16] and further improved in [21] based on introducing a new nonlinear state machine into the control loop. The dead zone can be effectively released and high power efficiency can be obtained with these methods. However, this work is based on the complicated theory and it is relatively difficult to apply in practical cost-sensitive fields.

Although many existing research works focus on the dead-zone mitigation methods, each method has its specific deriving theory. It is hard to find a general rule or a systematic principle to develop dead-zone mitigation methods in the literature. Therefore, this paper aims to analyze the relationship between the duty cycles of the active switches and the voltage conversion ratio of the converter from a novel perspective and to demystify the origin of the dead zone. Based on this, a series of multimode modulation schemes are systematically derived as the solutions to eliminate the dead-zone issue. The effect of different modulation modes on the inductor current ripple and the average value of the inductor, which is related to the efficiency of the converter [12], [22], is also investigated.

The remainder of this paper is arranged as follows. The voltage conversion ratio, and one-mode modulation and two-mode modulation methods are analyzed in Section II. Based on this, the origin of the dead zone is derived. Then, a series of dead-zone elimination methods are derived in Section III. To evaluate the performance of different modulation methods, the inductor current performance including the current ripple and the average value is investigated in Section IV. Two implementation examples of a four-mode modulation scheme are presented in Section V. Experimental results of the two implementation examples are carried out in Section VI to verify the effectiveness of the modulation scheme. Finally, the conclusion is drawn in Section VII.

II. Origin of the Dead Zone

A. Relationship Between the Input and the Output Voltage

The configuration of the converter is shown in Fig. 1. In terms of the voltage-second balance principle of the inductor, the relationship between the input voltage and output voltage of the converter can be derived as

$$V_o = \frac{d_1}{1-d_2} V_{\text{in}} \tag{1}$$

where V_o is the output voltage, V_{in} is the input voltage, and d_1 and d_2 are the duty cycles of the two active switches S_1 and S_2.

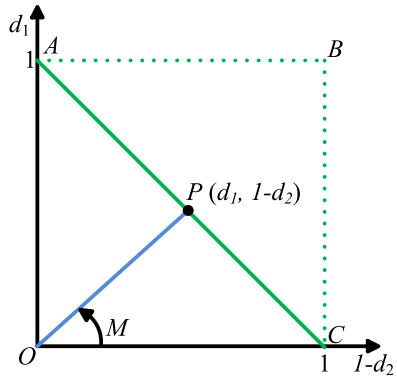

Fig. 2. One-mode modulation scheme.

It should be claimed that in order to simplify the analysis, all components are considered to be ideal components.

From (1), the voltage conversion ratio of the converter *M* can be obtained as

$$M = \frac{d_1}{1-d_2}. \tag{2}$$

Equations (1) and (2) show that there are two freedoms, i.e., d_1 and d_2, that can be used to regulate the voltage conversion ratio simultaneously or independently, which implies that there is a series of combination patterns of d_1 and d_2 that can be applied to achieve the desired output voltage from the input voltage. Equation (2) can be further clearly expressed as shown in Fig. 2, in which the vertical axis represents d_1, the horizontal axis represents $1-d_2$, and the slope of the line *OP*, which connects the origin *O* and the operating point *P*, represents the voltage conversion ratio. According to the location of the operating point *P*, different modulation schemes can be obtained, which are to be explained in detail in following sections.

B. One-Mode Modulation

Theoretically, the operating point *P* can be located at anywhere in the rectangle *ABCO* including the boundaries and the inner area. When the trajectory of the operating point *P* is located on the diagonal line of the rectangle, which is line *AC* as shown in Fig. 2, it can be seen that slope of the line *OP* can vary from zero to infinite. In this case, the voltage conversion ratio is continuous over the entire input voltage range and both duty cycles have a value in the range [0, 1], which means that both of the two active switches S_1 and S_2 are turned-ON/OFF in a single switching period. As the converter only operates in buck–boost mode under this modulation scheme, it is called one-mode modulation in this paper. This modulation method has been investigated experiencing low power conversion efficiency in the literature. Also, this modulation method will generate high inductor current ripple as well as high inductor current average value. Therefore, this modulation method is not expected in practical applications.

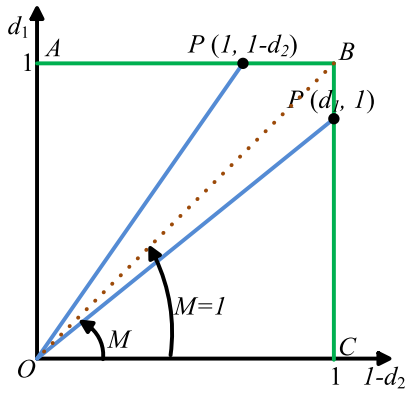

Fig. 3. Two-mode modulation scheme.

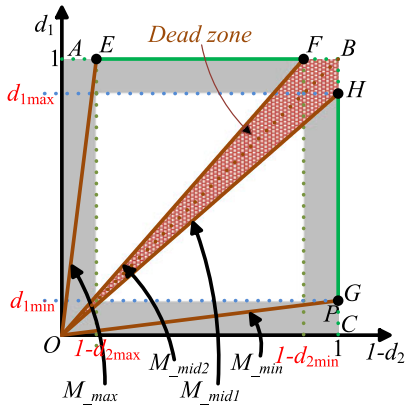

Fig. 4. Dead zone.

C. Two-Mode Modulation

When the trajectory of the operating point P is located only on the boundaries of the rectangle AB and CB as shown in Fig. 3, i.e., either d_1 or $1 - d_2$ is kept at 1, only one active switch is turned-ON/OFF in a single switching period. When the slope of the line OP is smaller than 1, which indicates that the input voltage is higher than the output voltage, $1 - d_2$ is kept at 1 while d_1 is controlled to regulate the output voltage and the converter operates in buck mode; when the slope of the line OP is greater than 1, which indicates that the input voltage is lower than the output voltage, d_1 is kept at 1 while d_2 is controlled to regulate the output voltage and the converter operates in boost mode. Therefore, this modulation scheme is called two-mode modulation in this paper. The two-mode modulation method is preferable in practical applications as it contributes to relatively higher efficiency and generates smaller inductor current ripple and inductor current average value compared to the one-mode modulation scheme.

D. Origin of the Dead Zone

Although the two-mode modulation can obtain high efficiency and better inductor current performance, there is an unneglectable drawback hidden in this modulation method. Due to the practical unavoidable nonidealities, switching noise, and other unpredictable disturbance of electronic components and the circuit layout, the duty cycle always has an upper limitation $d_{\_\max}$ and a lower limitation $d_{\_\min}$; therefore, d_1 and $1 - d_2$ can only achieve the values in the ranges EF and GH as shown in Fig. 4, which indicates that the voltage conversion ratio can only reach the values in the ranges $[M_{\_\min}, M_{\_\mathrm{mid1}}]$ and $[M_{\_\mathrm{mid2}}, M_{\_\max}]$ while the values in the ranges $[0, M_{\_\min}]$, $[M_{\_\max}, \infty]$, and $[M_{\_\mathrm{mid1}}, M_{\_\mathrm{mid2}}]$ are not achievable. The values in the ranges $[0, M_{\_\min}]$ and $[M_{\_\max}, \infty]$ are ignorable and can be avoided easily by designing the specification of the converter whereas the values in the range $[M_{\_\mathrm{mid1}}, M_{\_\mathrm{mid2}}]$ are essential for the converter as they need to be reached by the voltage conversion ratio when the input voltage approaches the output voltage. Therefore, the range $[M_{\_\mathrm{mid1}}, M_{\_\mathrm{mid2}}]$ is defined as dead zone as shown in the shadowed area in Fig. 4.

It can be seen that there are no trajectories for the operating point P when the converter operates in the dead zone. This fact results in the performance that the operating point P tends to jump between the point F and point B when the converter operates in boost mode and between the point H and point B when the converter operates in buck mode, which indicates that the voltage conversion ratio M jumps from $M_{\_\mathrm{mid1}}$ to 1 or vice versa when the input voltage is higher than the output voltage and from 1 to $M_{\_\mathrm{mid2}}$ or vice versa when the input voltage is lower than the output voltage. This phenomenon leads to the discontinuity of the voltage conversion ratio M and brings some negative effects on the performance of the converter such as the increase of the output voltage ripple, the appearance of subharmonics in the output voltage, and even the unstable and uncontrollable operation of the converter.

III. Multimode Modulation Method

In order to eliminate the dead zone, extra trajectories are demanded for the operating point P, which means that other operating modes are required to be inserted into the two-mode modulation scheme. Hence, multimode modulation schemes are required to be studied to implement the smooth mode transition between the buck mode and the boost mode. Basically, multimode modulation methods can be categorized into two types: three-mode modulation methods and four-mode modulation methods, which are to be analyzed in detail in the following sections.

A. Three-Mode Modulation

By inserting a straight line as the trajectory for the operating point P in the dead zone, three-mode modulation methods can be derived. Since the additional trajectory line can be adopted in different approaches, several three-mode modulation methods can be obtained. This section will describe three typical three-mode modulation schemes as examples.

1) Regulating Both d_1 and d_2 in the Dead Zone: The first choice to add the additional straight trajectory for the operating point P is to apply an oblique line DI, which is a part of the diagonal AC as shown in Fig. 5. When the input voltage approaches the output voltage, the converter will operate in the

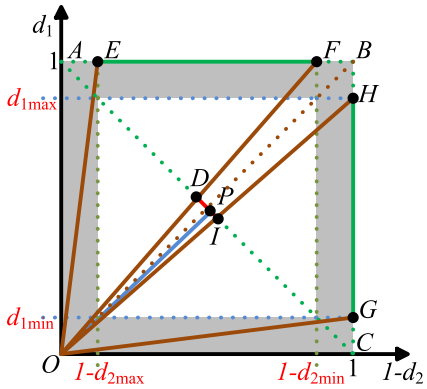

Fig. 5. Three-mode modulation scheme I.

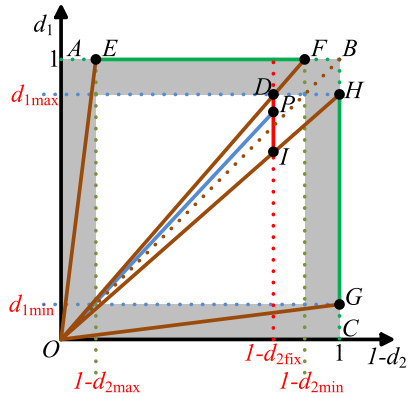

Fig. 6. Three-mode modulation scheme II.

buck–boost mode. In this case, both two active switches S_1 and S_2 are turned-ON/OFF in a single switching period. In this modulation method, the converter operates in buck mode when the input voltage is sufficiently higher than the output voltage, which implies that the voltage conversion ratio is in the range $[M_{\_\min}, M_{\_\mathrm{mid1}}]$; in boost mode when the input voltage is sufficiently lower than the input voltage, which implies that the voltage conversion ratio is in the range $[M_{\_\mathrm{mid2}}, M_{\_\max}]$; and in buck–boost mode when the input voltage is close to the output voltage, which implies that the voltage conversion ratio is in the range $[M_{\_\mathrm{mid1}}, M_{\_\mathrm{mid2}}]$.

The relationship between the duty cycles d_1 and d_2 when the voltage conversion ratio is in the range $[M_{\_\mathrm{mid1}}, M_{\_\mathrm{mid2}}]$ under this modulation scheme can be expressed as

$$d_1 = d_2. \tag{3}$$

2) Clamping d_2 and Regulating d_1 in the Dead Zone: The other choice to insert the straight additional trajectory for the operating point *P* is to apply a vertical line *DI* as shown in Fig. 6. When the input voltage approaches the output voltage, the duty cycle d_2 is clamped at a constant value $d_{2\mathrm{fix}}$, which is slightly higher than the minimum value $d_{2\min}$, while the duty cycle d_1 is controlled to regulate the output voltage. As this operating mode is similar to the buck mode, in which the duty cycle d_2 is clamped at zero while the duty cycle d_1 is regulated to obtain the desired output voltage, it is defined as extend-buck mode in this paper. In this modulation scheme, when the duty cycle d_1 reaches its maximum value in buck operating mode or the duty cycle d_2 reaches its minimum value in boost operating mode, the converter shifts to the extend-buck operating mode, the dead zone is, therefore, avoided.

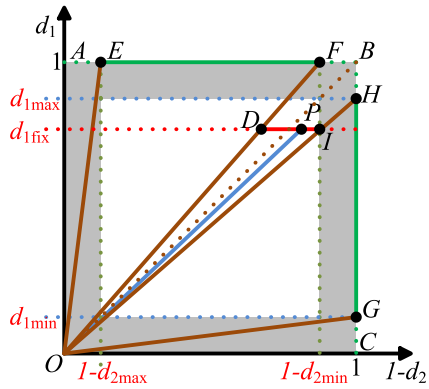

Fig. 7. Three-mode modulation scheme III.

The relationship between the duty cycles d_1 and d_2 when the voltage conversion ratio is in the range $[M_{\_\mathrm{mid1}}, M_{\_\mathrm{mid2}}]$ under this modulation scheme can be expressed as

$$\begin{cases} d_2 = d_{2\mathrm{fix}} \\ d_1 = \dfrac{v_o}{v_{\mathrm{in}}}(1 - d_{2\mathrm{fix}}) \\ d_{2\mathrm{fix}} = 1 - d_{1\max}(1 - d_{2\min}) \end{cases}. \tag{4}$$

3) Clamping d_1 and Regulating d_2 in the Dead Zone: Another choice to add the additional straight trajectory is to apply a horizontal line *DI* as shown in Fig. 7. When the input voltage is close to the output voltage, the duty cycle d_1 is clamped at a constant value $d_{1\mathrm{fix}}$, which is slightly lower than the maximum value $d_{1\max}$, while the duty cycle d_2 is controlled to regulate the output voltage. As this operating mode is similar to the boost mode, in which the duty cycle d_1 is clamped at one while the duty cycle d_2 is regulated to obtain the desired output voltage, it is defined as extend-boost mode in this paper. In this modulation scheme, when the duty cycle d_1 reaches its maximum value in buck operating mode or the duty cycle d_2 reaches its minimum value in boost operating mode, the converter shifts to the extend-boost mode, the dead zone is hence eliminated.

The relationship of the duty cycles d_1 and d_2 when the voltage conversion ratio falls in $[M_{\_\mathrm{mid1}}, M_{\_\mathrm{mid2}}]$ under this modulation scheme can be expressed as

$$\begin{cases} d_1 = d_{1\mathrm{fix}} \\ d_2 = 1 - \dfrac{v_{\mathrm{in}}}{v_o} d_{1\mathrm{fix}} \\ d_{1\mathrm{fix}} = d_{1\max}(1 - d_{2\min}) \end{cases}. \tag{5}$$

B. Four-Mode Modulation

By applying a polyline as the trajectory for the operating point *P* in the dead zone, four-mode modulation schemes can be deduced. As the additional polyline trajectory can be adopted in different approaches, different four-mode modulation methods

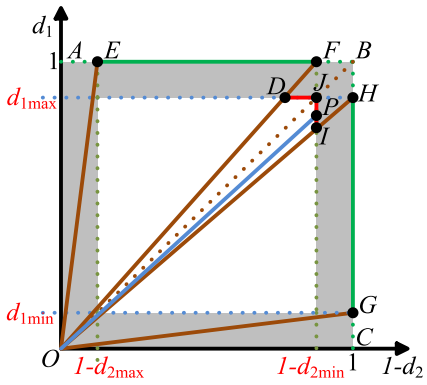

Fig. 8. Four-mode modulation scheme I.

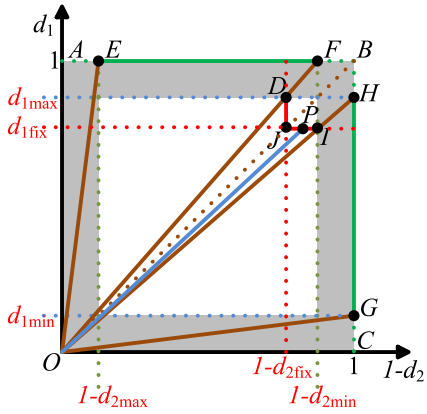

Fig. 9. Four-mode modulation scheme II.

can be obtained. Two typical four-mode modulation methods are to be analyzed as examples in this section.

1) Clamping d_1 at Its Maximum Value and Clamping d_2 at Its Minimum Value: Through inserting a convex polyline *DJI* as the additional trajectory for the operating point *P* as shown in Fig. 8, a four-mode modulation method can be obtained. Similar as three-mode modulation schemes, when the input voltage is sufficiently higher or lower than the output voltage, the converter operates in the buck and the boost modes, respectively. When the input voltage is close to the output voltage, the converter will operate in two different modes, which are the extend-buck mode and the extend-boost mode represented by the trajectories *IJ* and *DJ*, respectively. When the input voltage is slightly higher than the output voltage, which means that the voltage conversion ratio is in the range $[M_{\_\text{mid1}},\ 1]$, the operating point *P* will move on the vertical trajectory line *IJ* and the converter operates in extend-buck mode. In this operating mode, the duty cycle d_2 is clamped at its minimum value $d_{2\text{min}}$ while the duty cycle d_1 is controlled to regulate the output voltage. When the input voltage is slightly lower than the output voltage, which means that the voltage conversion ratio is in the range $[1,\ M_{\_\text{mid2}}]$, the operating point *P* will move on the horizontal trajectory line *DJ* and the converter operates in extend-boost mode. In this operating mode, the duty cycle d_1 is clamped at its maximum value $d_{1\text{max}}$ while the duty cycle d_2 is controlled to regulate the output voltage. Through inserting the extend-buck mode and the extend-boost operating mode, the elimination of the dead zone can be implemented.

The relationship between the duty cycles d_1 and d_2 when the voltage conversion ratio is in the range $[M_{\_\text{mid1}},\ M_{\_\text{mid2}}]$ under this modulation scheme can be expressed as

$$\begin{cases} d_1 = \dfrac{v_o}{v_{\text{in}}}(1-d_{2\text{min}}), d_2 = d_{2\text{min}} & M \in [M_{\_\text{mid1}}, 1] \\ d_1 = d_{1\text{max}}, d_2 = 1 - \dfrac{v_{\text{in}}}{v_o} d_{1\text{max}} & M \in [1, M_{\_\text{mid2}}] \end{cases}. \tag{6}$$

2) Clamping d_1 at a Fixed Value That is Lower Than Its Maximum Value and Clamping d_2 at a Fixed Value That is Higher Than Its Minimum Value: By inserting a concave polyline *DJI* as the additional trajectory for the operating point *P* as shown in Fig. 9, another four-mode modulation method can be derived. When the input voltage is sufficiently higher or lower than the output voltage, the converter has the same operating principle as the previously described four-mode modulation method; while when the input voltage is close to the output voltage, the converter has different operating processes. When the input voltage is slightly higher than the output voltage, which means that the voltage conversion ratio is in the range $[M_{\_\text{mid1}},\ 1]$, the operating point *P* will move on the horizontal trajectory line *IJ* and the converter operates in extend-boost mode. In this operating mode, the duty cycle d_1 is clamped at a constant value $d_{1\text{fix}}$, which is slightly smaller than its maximum value $d_{1\text{max}}$, and the duty cycle d_2 is controlled to regulate the output voltage. When the input voltage is slightly lower than the output voltage, which means that the voltage conversion ratio is in the range $[1,\ M_{\_\text{mid2}}]$, the operating point *P* will move on the vertical trajectory line *DJ* and the converter operates in extend-buck mode. In this operating mode, the duty cycle d_2 is clamped at a constant value $d_{2\text{fix}}$, which is slightly higher than its minimum value $d_{2\text{min}}$, and the duty cycle d_1 is controlled to regulate the output voltage. Therefore, when the voltage conversion ratio is located in the range $[M_{\_\text{mid1}},\ M_{\_\text{mid2}}]$, extend-buck and extend-boost modes can be applied to implement the elimination of the dead zone and smooth transition between the buck mode and boost mode.

The relationship between the duty cycles d_1 and d_2 when the voltage conversion ratio is in the range $[M_{\_\text{mid1}},\ M_{\_\text{mid2}}]$ under this modulation scheme can be expressed as

$$\begin{cases} d_1 = d_{1\text{fix}}, d_2 = 1 - \dfrac{v_{\text{in}}}{v_o} d_{1\text{fix}} & M \in [M_{\_\text{mid1}}, 1] \\ d_{1\text{fix}} = d_{1\text{max}}(1-d_{2\text{min}}) & \\ d_1 = \dfrac{v_o}{v_{\text{in}}}(1-d_{2\text{fix}}), d_2 = d_{2\text{fix}} & M \in [1, M_{\_\text{mid2}}] \\ d_{2\text{fix}} = 1 - d_{1\text{max}}(1-d_{2\text{min}}) & \end{cases}. \tag{7}$$

IV. Study of the Inductor Current Performance Under Different Modulation Schemes

It is known that the amount of the power loss determines the efficiency of the converter. For the noninverting synchronous buck–boost converter, the core loss of the inductor and the

conduction loss contribute most of the total power loss [22]. It is investigated that the inductor core loss is related to the inductor current ripple [22], while the conduction loss is related to the inductor current root-mean-square value, which is similar to the average value when the current ripple is small [12]. Therefore, this section is to study the inductor current ripple and average value of the converter under the proposed different modulation schemes.

When the converter operates under one-mode modulation scheme, the inductor current ripple $I_{\mathrm{rip\_1mode}}$ and the average value $I_{\mathrm{avg\_1mode}}$ can be expressed, respectively, over the entire input voltage range:

$$I_{\mathrm{rip\_1mode}} = \frac{V_{\mathrm{in}} V_o}{L f_s (V_o + V_{\mathrm{in}})} \tag{8}$$

$$I_{\mathrm{avg\_1mode}} = \frac{V_o + V_{\mathrm{in}}}{V_{\mathrm{in}}} I_o \tag{9}$$

where V_{in} is the input voltage, V_o is the output voltage, L is the inductance of the inductor, f_s is the switching frequency, and I_o is the output current.

When the converter operates under the two-mode modulation scheme, the inductor current ripple $I_{\mathrm{rip\_2mode}}$ and the average value $I_{\mathrm{avg\_2mode}}$ can be expressed as

$$I_{\mathrm{rip\_2mode}} = \begin{cases} \dfrac{V_{\mathrm{in}}(V_o - V_{\mathrm{in}})}{L f_s V_o} & V_{\mathrm{in}} \le V_o \\ \dfrac{V_o(V_{\mathrm{in}} - V_o)}{L f_s V_{\mathrm{in}}} & V_{\mathrm{in}} > V_o \end{cases} \tag{10}$$

$$I_{\mathrm{avg\_2mode}} = \begin{cases} \dfrac{V_o}{V_{\mathrm{in}}} I_o & V_{\mathrm{in}} \le V_o \\ I_o & V_{\mathrm{in}} > V_o \end{cases}. \tag{11}$$

When the converter operates under the three-mode modulation scheme I, the inductor current ripple $I_{\mathrm{rip\_3modeI}}$ and the average value $I_{\mathrm{avg\_3modeI}}$ can be expressed as

$$I_{\mathrm{rip\_3modeI}} = \begin{cases} \dfrac{V_{\mathrm{in}}(V_o - V_{\mathrm{in}})}{L f_s V_o} & V_{\mathrm{in}} \le V_{\mathrm{fix1}} \\ \dfrac{V_{\mathrm{in}} V_o}{L f_s (V_{\mathrm{in}} + V_o)} & V_{\mathrm{fix1}} < V_{\mathrm{in}} \le V_{\mathrm{fix2}} \\ \dfrac{V_o(V_{\mathrm{in}} - V_o)}{L f_s V_{\mathrm{in}}} & V_{\mathrm{in}} > V_{\mathrm{fix2}} \end{cases} \tag{12}$$

$$I_{\mathrm{avg\_3modeI}} = \begin{cases} \dfrac{V_o}{V_{\mathrm{in}}} I_o & V_{\mathrm{in}} \le V_{\mathrm{fix1}} \\ \dfrac{V_o + V_{\mathrm{in}}}{V_{\mathrm{in}}} I_o & V_{\mathrm{fix1}} < V_{\mathrm{in}} \le V_{\mathrm{fix2}} \\ I_o & V_{\mathrm{in}} > V_{\mathrm{fix2}} \end{cases} \tag{13}$$

where $V_{\mathrm{fix1}} = V_o / M_{\mathrm{mid2}}$ and $V_{\mathrm{fix2}} = V_o / M_{\mathrm{mid1}}$.

When the converter operates under the three-mode modulation scheme II, the inductor current ripple $I_{\mathrm{rip\_3modeII}}$ and the average value $I_{\mathrm{avg\_3modeII}}$ can be expressed as

$$I_{\mathrm{rip\_3modeII}} = \begin{cases} \dfrac{V_{\mathrm{in}}(V_o - V_{\mathrm{in}})}{L f_s V_o} & V_{\mathrm{in}} \le V_{\mathrm{fix1}} \\ \dfrac{V_{\mathrm{in}} d_{2\mathrm{fix}}}{L f_s} & V_{\mathrm{fix1}} < V_{\mathrm{in}} \le V_o \\ \dfrac{V_o(V_{\mathrm{in}} - V_o(1 - d_{2\mathrm{fix}}))}{L f_s V_{\mathrm{in}}} & V_o < V_{\mathrm{in}} \le V_{\mathrm{fix2}} \\ \dfrac{V_o(V_{\mathrm{in}} - V_o)}{L f_s V_{\mathrm{in}}} & V_{\mathrm{in}} > V_{\mathrm{fix2}} \end{cases} \tag{14}$$

$$I_{\mathrm{avg\_3modeII}} = \begin{cases} \dfrac{V_o}{V_{\mathrm{in}}} I_o & V_{\mathrm{in}} \le V_{\mathrm{fix1}} \\ \dfrac{1}{1 - d_{2\mathrm{fix}}} I_o & V_{\mathrm{fix1}} < V_{\mathrm{in}} \le V_o \\ \dfrac{1}{1 - d_{2\mathrm{fix}}} I_o & V_o < V_{\mathrm{in}} \le V_{\mathrm{fix2}} \\ I_o & V_{\mathrm{in}} > V_{\mathrm{fix2}} \end{cases}. \tag{15}$$

When the converter operates under the three-mode modulation scheme III, the inductor current ripple $I_{\mathrm{rip\_3modeIII}}$ and the average value $I_{\mathrm{avg\_3modeIII}}$ can be expressed as

$$I_{\mathrm{rip\_3modeIII}} = \begin{cases} \dfrac{V_{\mathrm{in}}(V_o - V_{\mathrm{in}})}{L f_s V_o} & V_{\mathrm{in}} \le V_{\mathrm{fix1}} \\ \dfrac{V_{\mathrm{in}}(V_o - V_{\mathrm{in}} d_{1\mathrm{fix}})}{L f_s V_o} & V_{\mathrm{fix1}} < V_{\mathrm{in}} \le V_o \\ \dfrac{V_o(1 - d_{1\mathrm{fix}})}{L f_s} & V_o < V_{\mathrm{in}} \le V_{\mathrm{fix2}} \\ \dfrac{V_o(V_{\mathrm{in}} - V_o)}{L f_s V_{\mathrm{in}}} & V_{\mathrm{in}} > V_{\mathrm{fix2}} \end{cases} \tag{16}$$

$$I_{\mathrm{avg\_3modeIII}} = \begin{cases} \dfrac{V_o}{V_{\mathrm{in}}} I_o & V_{\mathrm{in}} \le V_{\mathrm{fix1}} \\ \dfrac{V_o}{V_{\mathrm{in}} d_{1\mathrm{fix}}} I_o & V_{\mathrm{fix1}} < V_{\mathrm{in}} \le V_o \\ \dfrac{V_o}{V_{\mathrm{in}} d_{1\mathrm{fix}}} I_o & V_o < V_{\mathrm{in}} \le V_{\mathrm{fix2}} \\ I_o & V_{\mathrm{in}} > V_{\mathrm{fix2}} \end{cases}. \tag{17}$$

When the converter operates under the four-mode modulation scheme I, the inductor current ripple $I_{\mathrm{rip\_4modeI}}$ and the average value $I_{\mathrm{avg\_4modeI}}$ can be expressed as

$$I_{\mathrm{rip\_4modeI}} = \begin{cases} \dfrac{V_{\mathrm{in}}(V_o - V_{\mathrm{in}})}{L f_s V_o} & V_{\mathrm{in}} \le V_{\mathrm{fix1}} \\ \dfrac{V_{\mathrm{in}}(V_o - V_{\mathrm{in}} d_{1\max})}{L f_s V_o} & V_{\mathrm{fix1}} < V_{\mathrm{in}} \le V_o \\ \dfrac{V_o(V_{\mathrm{in}} - V_o(1 - d_{2\min}))}{L f_s V_{\mathrm{in}}} & V_o < V_{\mathrm{in}} \le V_{\mathrm{fix2}} \\ \dfrac{V_o(V_{\mathrm{in}} - V_o)}{L f_s V_{\mathrm{in}}} & V_{\mathrm{in}} > V_{\mathrm{fix2}} \end{cases} \tag{18}$$

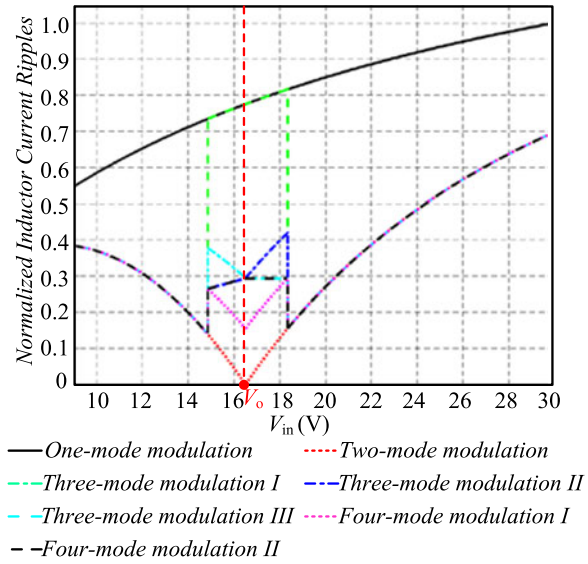

Fig. 10. Normalized inductor current ripples under different modulation schemes.

$$I_{\text{avg\_4modeI}} = \begin{cases} \dfrac{V_o}{V_{\text{in}}} I_o & V_{\text{in}} \le V_{\text{fix1}} \\ \dfrac{V_o}{V_{\text{in}} d_{1\max}} I_o & V_{\text{fix1}} < V_{\text{in}} \le V_o \\ \dfrac{1}{1-d_{2\min}} I_o & V_o < V_{\text{in}} \le V_{\text{fix2}} \\ I_o & V_{\text{in}} > V_{\text{fix2}} \end{cases}. \quad (19)$$

When the converter operates under the four-mode modulation scheme II, the inductor current ripple $I_{\text{rip\_4modeII}}$ and the average value $I_{\text{avg\_4modeII}}$ can be expressed as

$$I_{\text{rip\_4modeII}} = \begin{cases} \dfrac{V_{\text{in}}(V_o - V_{\text{in}})}{L f_s V_o} & V_{\text{in}} \le V_{\text{fix1}} \\ \dfrac{V_{\text{in}} d_{2\text{fix}}}{L f_s} & V_{\text{fix1}} < V_{\text{in}} \le V_o \\ \dfrac{V_o(1-d_{1\text{fix}})}{L f_s} & V_o < V_{\text{in}} \le V_{\text{fix2}} \\ \dfrac{V_o(V_{\text{in}} - V_o)}{L f_s V_{\text{in}}} & V_{\text{in}} > V_{\text{fix2}} \end{cases} \quad (20)$$

$$I_{\text{avg\_4modeII}} = \begin{cases} \dfrac{V_o}{V_{\text{in}}} I_o & V_{\text{in}} \le V_{\text{fix1}} \\ \dfrac{1}{1-d_{2\text{fix}}} I_o & V_{\text{fix1}} < V_{\text{in}} \le V_o \\ \dfrac{V_o}{V_{\text{in}} d_{1\text{fix}}} I_o & V_o < V_{\text{in}} \le V_{\text{fix2}} \\ I_o & V_{\text{in}} > V_{\text{fix2}} \end{cases}. \quad (21)$$

In order to clearly show the comparison among the inductor current ripples of the converter under different modulation schemes, the normalized current ripples are sketched in Fig. 10 by taking the maximum value of the current ripple under the one-mode modulation scheme $I_{\text{rip}_1\text{mode\_max}}$, which can be obtained when the input voltage is at the highest value as shown in the following equation, as the base:

$$I_{\text{rip\_1mode\_max}} = \frac{V_{\text{in\_max}} V_o}{L f_s (V_o + V_{\text{in\_max}})}. \quad (22)$$

The parameters used to plot the figures are set as $V_{\text{in}} =$ 9-30 V, $V_o = 16.5$ V, $L = 10\,\mu$H, $P_o = 36$ W, and $f_s =$ 200 kHz. Since it has been reported that the maximum and minimum limitations of the duty cycles are around 0.9 and 0.1, respectively [10], [17], [20], the limitations of the duty cycles used in this study are assumed as $d_{1\max} = 0.9$ and $d_{2\min} = 0.1$, then $d_{1\text{fix}}$ and $d_{2\text{fix}}$ can be calculated as $d_{1\text{fix}} = 0.81$ and $d_{2\text{fix}} \approx 0.19$ according to (4) and (5).

Fig. 10 shows that the inductor current ripple under the one-mode modulation scheme is the largest while the one under the two-mode modulation scheme is the smallest. The inductor current ripples under all three-mode and four-mode modulation schemes are the same as those under the two-mode modulation scheme when the input voltage is sufficiently higher or lower than the output voltage. When the voltage is slightly higher than the output voltage, the inductor current ripple under the four-mode modulation scheme I is smaller than the ones under other three/four-mode modulation schemes while the one under the three-mode modulation scheme I is larger than the ones under other three/four-mode modulation schemes. The inductor current ripples under the three-mode modulation scheme II and the four-mode modulation scheme II are the same, which is lower than the one under the three-mode modulation scheme III and higher than the one under the four-mode modulation scheme I. When the voltage is slightly lower than the output voltage, the inductor current ripple under the four-mode modulation scheme I is still the smallest and the one under the three-mode modulation scheme I is still the largest among the ones under all three/four-mode modulation schemes. The inductor current ripples under the three-mode modulation scheme III and the four-mode modulation scheme II are the same, which is lower than the one under the three-mode modulation scheme II and higher than the one under the four-mode modulation scheme I.

The comparison among the normalized average values of the inductor current of the converter under different modulation schemes is depicted in Fig. 11 by taking the maximum value of the inductor current average value under the one-mode modulation scheme $I_{\text{avg\_1mode\_max}}$ as the base. $I_{\text{avg\_1mode\_max}}$ can be expressed as

$$I_{\text{avg\_1mode\_max}} = \frac{V_o + V_{\text{in\_min}}}{V_{\text{in\_min}}} I_o. \quad (23)$$

Fig. 11 shows that the average value of the inductor current under different modulation schemes has the same trend as the inductor current ripples over the entire input voltage range.

V. Implementation of Four-Mode Modulation I

As discussed in Section III, the dead zone can be mitigated by inserting an extend-buck mode or/and an extend-boost mode.

In the extend-buck mode, the duty cycle d_2 is clamped at a constant value that is its minimum value or a value slightly

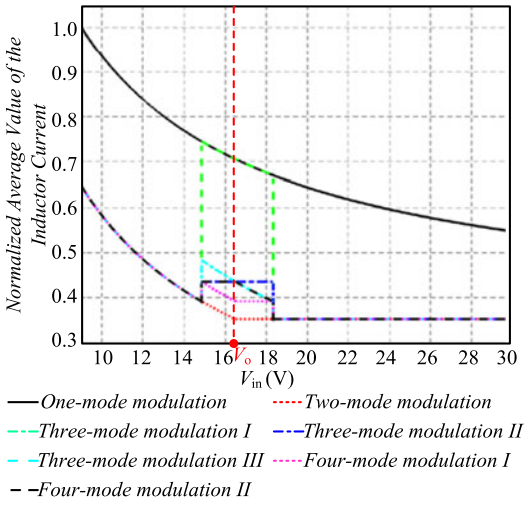

Fig. 11. Normalized average value of the inductor current under different modulation schemes.

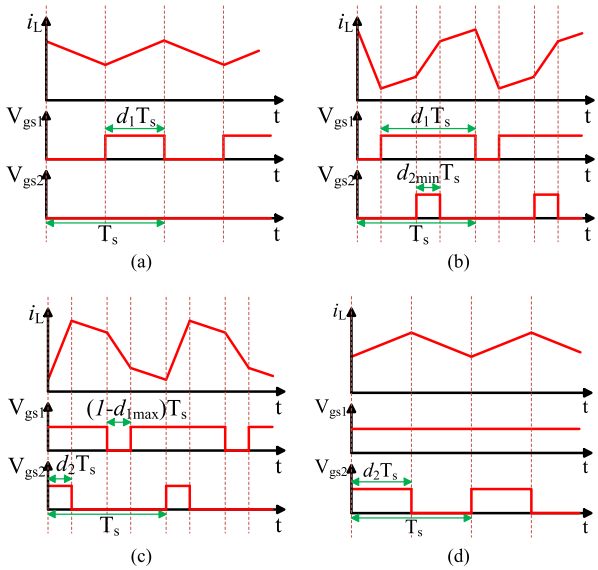

Fig. 12. Some key waveforms of the converter in different operating modes of the implementation example A, (a) buck mode, (b) extend-buck mode, (c) extend-boost mode, and (d) boost mode.

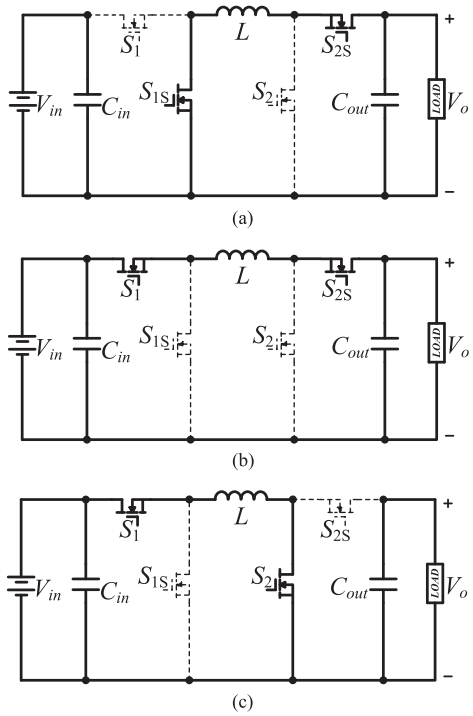

Fig. 13. Equivalent circuits of the converter in different operating stages.

higher than its minimum value, which means that the active switch S_2 will be turned-ON for a fixed time interval in a switching period. The turned-ON time of the switch S_2 can be at the beginning, in the middle, or the end of a switching period. In other words, this operating mode can be viewed as that the input voltage is boosted to a fixed relatively higher value before it is bucked to the desired output voltage to ensure the duty cycle d_1 being in the reachable range.

When the converter shifts to operate in extend-boost mode, the duty cycle d_1 is clamped at a constant value that is its maximum value or a value slightly lower than its maximum value, which means that the active switch S_1 will be turned-OFF for a fixed time interval in a switching period. The switch S_1 can be turned OFF at the beginning, in the middle, or the end of a switching period. In other words, this operating mode can be viewed as that the input voltage is bucked to a fixed relatively lower value before it is boosted to the desired output voltage to ensure the duty cycle d_2 being in the reachable range.

Depending on the turned-ON time of the switch S_2 in the extend-buck mode and the turned-OFF time of the switch S_1 in the extend-boost operating mode, several control methods can be applied to implement the multimode modulation schemes.

As two examples, two implementations of the four-mode modulation scheme I will be presented in this section. Similar approaches can be applied to implement previously analyzed other three/four-mode modulation schemes.

A. Turning ON the Switch S_2 in the Extend-Buck Mode and Turning OFF the Switch S_1 in the Extend-Boost Mode in the Middle of a Switching Period

In this implementation, the converter can operate in four modes, which are buck mode, boost mode, extend-buck mode, and extend-boost mode. Some key waveforms of the components are shown in Fig. 12. When the converter operates in the buck mode and the boost mode, the waveforms are shown in Fig. 12(a) and (d), which are the same as the buck converter and the boost converter, respectively; therefore, the detailed operating processes will not be analyzed in this paper.

When the converter operates in extend-buck mode, there are four operating stages. The waveforms in the four operating stages are shown in Fig. 12(b). In operating stage 1, the equivalent circuit of the converter is shown in Fig. 13(a). The switch S_1 (S_{1S}) is turned OFF (ON) and the switch S_2 (S_{2S}) is turned OFF (ON) as well, and the inductor current is decreasing. The equivalent circuit of the converter in operating stage 2 is shown in Fig. 13(b). In this operating stage, the switch S_1 (S_{1S}) is

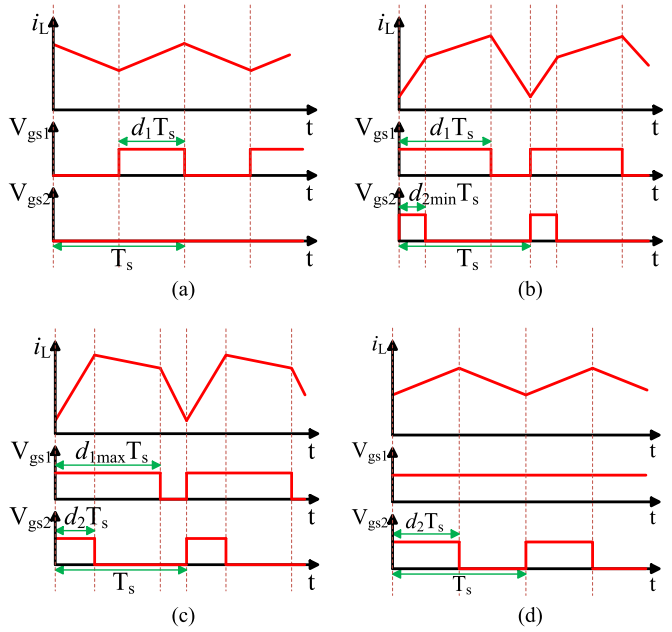

Fig. 14. Some main key waveforms of the converter in different operating modes of the implementation example B, (a) buck mode, (b) extend-buck mode, (c) extend-boost mode, and (d) boost mode.

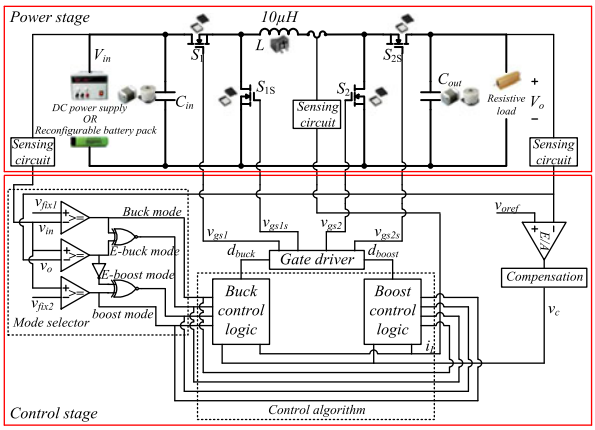

Fig. 15. Simplified block diagram of the experimental environment.

TABLE I
PARAMETERS OF THE COMPONENTS AND SPECIFICATIONS OF THE PROTOTYPES

Components	Type
MOSFETs S_1, S_{1S}, S_2, S_{2S}	SIR882DP-T1-GE3
Inductor L	10 μH
Input filter capacitor C_{in}	2 $*$ 47 μF Aluminum Electrolytic capacitors and 2 $*$ 4.7 μF ceramic capacitors connected in parallel
Output capacitor C_o	2 $*$ 220 μF Aluminum electrolytic capacitors and 2 $*$ 4.7 μF ceramic capacitors connected in parallel
Input voltage V_{in}	9–30 V
Output voltage V_o	16.5 V
Rated power	36 W
Switching frequency f_s	200 kHz

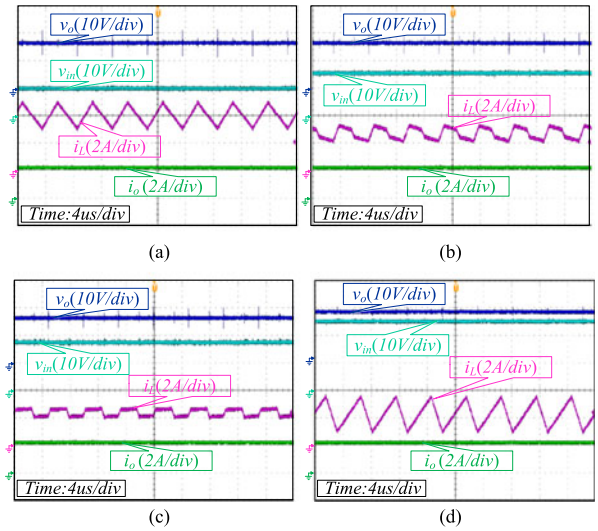

Fig. 16. Waveforms of the inductor current, the input voltage, and the output voltage of the implementation example A, (a) boost mode, (b) extend-boost mode, (c) extend-buck mode, and (d) buck mode.

turned ON (OFF) and the switch S_2 (S_{2S}) is still turned OFF (ON) till the middle of the switching period. Then, the converter shifts to operate in operating stage 3, the equivalent circuit is shown in Fig. 13(c). The switches S_1 and S_2 are both turned ON while the switches S_{1S} and S_{2S} are turned OFF, and the inductor current is increasing. Operating stage 3 ends at the time $(0.5 + d_{2\min})T_s$ (T_s is the switching period), which is the start of the operating stage 4. The operation principle in the operating stage 4 is the same as that in the operating stage 2. This operating stage will last until the end of the switching period.

When the converter operates in the extend-boost mode, there are also four operating stages. The waveforms in the four operating stages are shown in Fig. 12(c). During the operating stage 1, the equivalent circuit of the converter is shown in Fig. 13(c). The switch S_1 (S_{1S}) is turned ON (OFF) and the switch S_2 (S_{2S}) is turned ON (OFF) as well, and the inductor current is increasing. The equivalent circuit of the converter in operating stage 2 is shown in Fig. 13(b). In this operating stage, the switch S_1 (S_{1S}) is turned ON (OFF) and the switch S_2 (S_{2S}) is turned OFF (ON) till the middle of the switching period. Then, the converter shifts to operate in the operating stage 3, the equivalent circuit is shown in Fig. 13(a). The switch S_1 (S_{1S}) is turned OFF (ON) and the switch S_2 (S_{2S}) is turned OFF (ON), and the inductor current is decreasing. This operating stage ends at the time $(1.5 - d_{1\max})T_s$, which is the beginning of the operating stage 4. The operation principle in the operating stage 4 is the same as that in the operating stage 2. This operating stage will last till the end of the switching period.

B. Turning ON the Switch S_2 in the Extend-Buck Mode at the Beginning and Turning OFF the Switch S_1 in the Extend-Boost Mode Both at the End of a Switching Period

The converter will operate in four modes including buck mode, boost mode, extend-buck mode, and extend-boost mode in this implementation according to the relationship between the input voltage and the output voltage. Some key waveforms of the components are shown in Fig. 14. When the converter operates in the buck mode and the boost mode, the waveforms

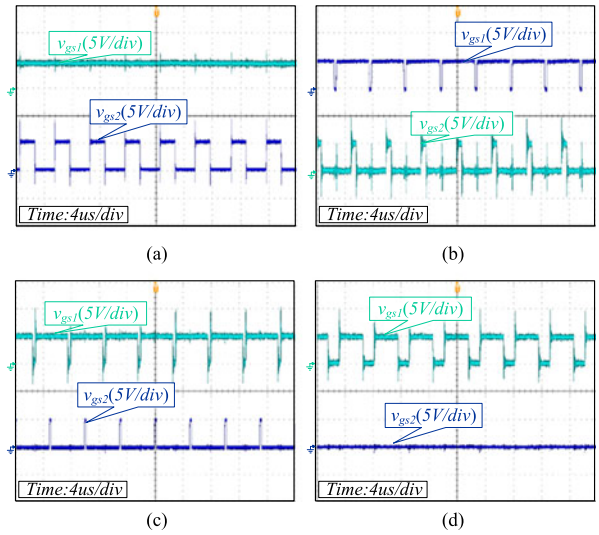

Fig. 17. Waveforms of the driving signals of the implementation example A, (a) boost mode, (b) extend-boost mode, (c) extend-buck mode, and (d) buck mode.

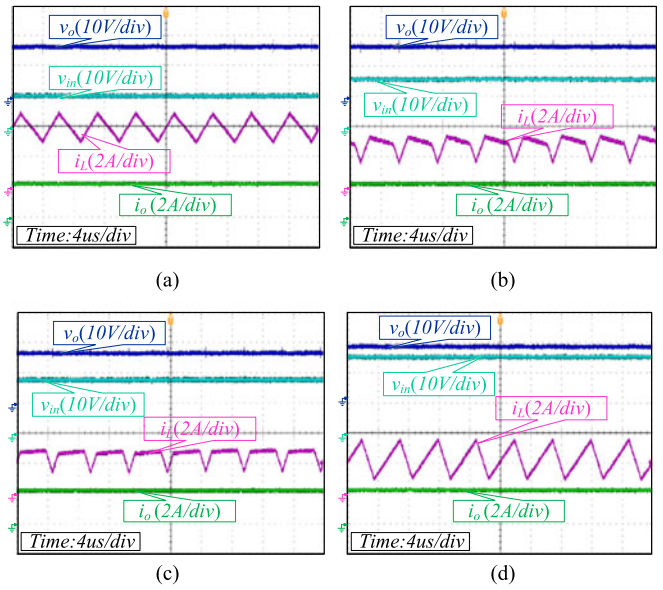

Fig. 18. Waveforms of the inductor current, the input voltage, and the output voltage of the implementation example B, (a) boost mode, (b) extend-boost mode, (c) extend-buck mode, and (d) buck mode.

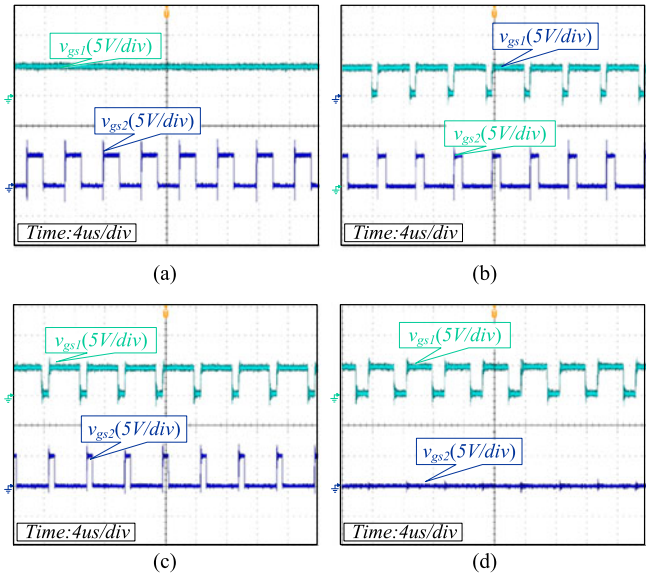

Fig. 19. Waveforms of the driving signals of the implementation example B, (a) boost mode, (b) extend-boost mode, (c) extend-buck mode, and (d) buck mode.

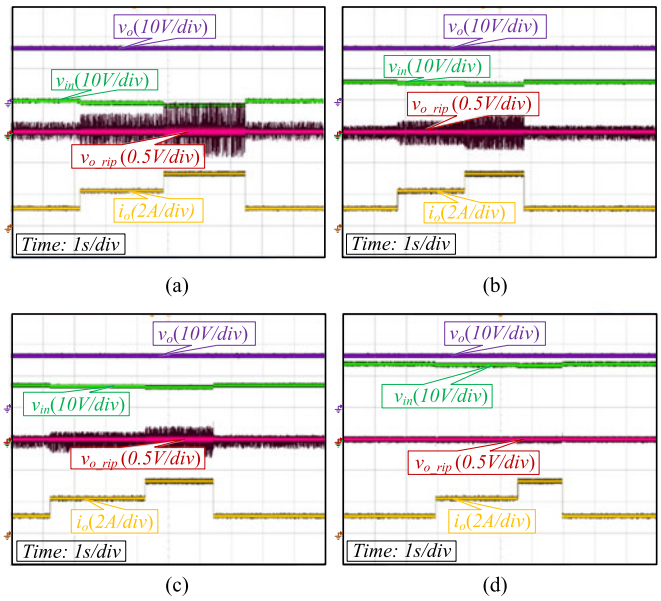

Fig. 20. Waveforms of load change under different operating modes, (a) $V_{\rm in}$ = 10 V, (b) $V_{\rm in}$ = 16 V, (c) $V_{\rm in}$ = 17.5 V, and (d) $V_{\rm in}$ = 24 V.

are shown in Fig. 14(a) and (d), which are the same as buck and boost converters, respectively; therefore, the detailed operating processes will not be analyzed in this paper.

When the converter operates in the extend-buck mode, there are three operating stages. The waveforms in the three operating stages are shown in Fig. 14(b). In operating stage 1, the equivalent circuit of the converter is shown in Fig. 13(c). The switch S_1 and switch S_2 are both turned ON while the switch S_{1S} and S_{2S} are turned OFF and the inductor current is increasing. Operating stage 1 ends at the time $d_{2\min}T_s$, which is the start of the operating stage 2. In operating stage 2, the equivalent circuit of the converter is shown in Fig. 13(b). The switch S_1 (S_{1S}) is still turned ON (OFF) while the switch S_2 (S_{2S}) is turned OFF (ON) in this stage. In operating stage 3, both of the switches S_1 and S_2 are turned OFF and the inductor current is decreasing till the end of the switching period.

When the converter operates in the extend-boost mode, there are also three operating stages. The waveform in the three operating stages is shown in Fig. 14(c). In operating stage 1, the equivalent circuit of the converter is shown in Fig. 13(c). The switches S_1 and S_2 are both turned ON and the inductor current is increasing. In operating stage 2, the equivalent circuit of the converter is shown in Fig. 13(b). The switch S_1 is still turned ON while the switch S_2 is turned OFF. This operating stage ends at the time $d_{1\max}T_s$, which is the shifting time from stage 2 to

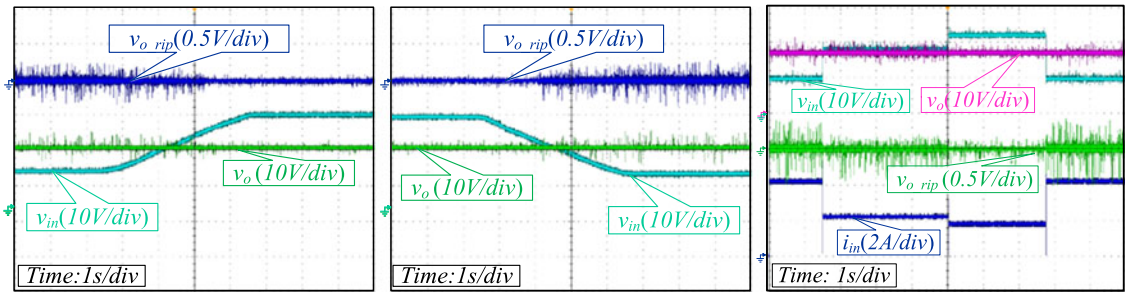

Fig. 21. Waveforms of input voltage change under different load conditions, (a) input voltage increases smoothly, (b) input voltage decreases smoothly, and (c) input voltage experiences sudden change.

stage 3. In operating stage 3, both of the switches S_1 and S_2 are turned OFF and the inductor current is decreasing till the end of the switching period.

VI. Experimental Results

To show the applicability of the proposed strategies under different conditions, two prototypes have been built and tested to verify the effectiveness of the two implementations presented in Section V accordingly. The experimental environment of the two prototypes is the same and a simplified block diagram of the experimental environment is shown in Fig. 15. It should be claimed that different control methods such as voltage mode control methods and current mode control methods can all be used as the control algorithm to implement the proposed modulation schemes in practical applications and some control algorithm concepts have been studied in the literature [7], [12]–[14], [17], [18]. With the benefits of improved transient response, satisfied output immunity to the input variance, self-protection against over current, and easiness for parallel operating of several converters, the current programmed control method investigated in [18] is adopted in this study. The components used in the two prototypes are listed in Table I. A reconfigurable battery pack using the NCR18650PF Li-ion batteries is used to test the dynamical performance of the converter when the input voltage experiences sudden changes and a dc power supply is used for other tests. The waveforms are recorded by the oscilloscope Tektronix MDO3024.

Fig. 16 shows the waveforms of the input voltage, the output voltage, and the inductor current while Fig. 17 shows the switching sequences of the four switches of the implementation example A. The waveforms of the input voltage, the output voltage, and the inductor current of the implementation example B are shown in Fig. 18 while the switching sequences of the four switches are shown in Fig. 19. It can be seen that the waveforms of the two prototypes are all corresponding well with the theoretical analysis.

In order to demonstrate the dynamical performance of the converter with the proposed modulation strategies, some tests with variation of the input voltage and load condition have been worked out for the two prototypes. The measured results from the implementation example A are shown in Figs. 20 and 21. Fig. 20 shows the waveforms of the output voltage when the load suddenly changes under different input voltage conditions. It

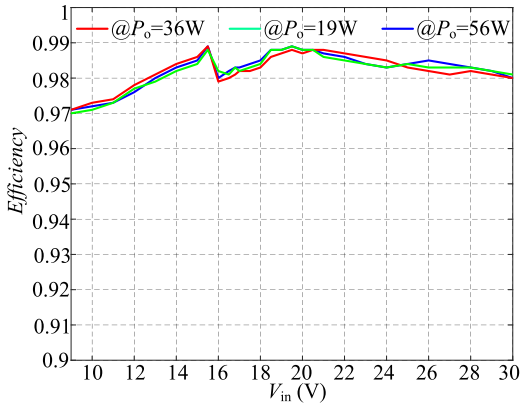

Fig. 22. Efficiency of the implementation example A.

can be seen that the output voltage remains highly stable during the change of the load condition and the output voltage ripple increases slightly with the increase of the output power under all input voltage conditions. Note that the input voltage sees a slight change according to the change of the load condition; this is the effect caused by the internal resistance of the input source. The waveforms indicate that the load transient response of the converter with the proposed four-mode modulation scheme I is satisfactory.

Fig. 21 shows the waveforms of the output voltage and output voltage ripples when the input voltage experiences smooth and sudden changes. It can be seen that the output voltage is stable during the transient period under all input voltage changing conditions. Hence, the satisfied input voltage transient response of the converter is verified. As similar transient performance has been obtained for the implementation example B, hence they are not presented in this paper. The experimental results well demonstrate the effectiveness of the four-mode modulation scheme I.

Fig. 22 shows the power conversion efficiency of the implementation example A versus the input voltage under three different load conditions. It can be seen that the converter with the four-mode control method can obtain over 97% efficiency in the entire input voltage range under all load conditions. The power conversion efficiency of the implementation example B reaches over 96% in the experiment. The results demonstrate

that the noninverting buck–boost converter can obtain satisfied efficiency with the proposed dead-zone elimination strategies.

VII. Conclusion

The origin of the dead zone hidden in the high-efficiency two-mode modulation scheme of the noninverting synchronous buck–boost converter is analyzed in this paper. Based on this, a series of three-mode and four-mode modulation schemes are derived systematically to eliminate the dead zone. The inductor performance under different modulation schemes is analyzed and compared as an evaluation for these modulation methods. Two implementation examples of the four-mode modulation scheme I proposed in this paper are presented and verified by experimental results in this paper. This paper can be an appropriate guidance for developing new control methods to implement smooth mode transition and high efficiency operation of the noninverting synchronous buck–boost converter in practical applications that require a fixed output voltage while in the face of the input voltage varying in a wide range.

References

[1] Y. J. Lee, A. Khaligh, A Chakraborty, and A. Emadi, "Digital combination of buck and boost converters to control a positive buck–boost converter and improve the output transients," *IEEE Trans. Power Electron.*, vol. 24, no. 5, pp. 1267–1279, May 2009.

[2] C. Yao, X. Ruan, W. Cao, and P. Chen, "A two-mode control scheme with input voltage feed-forward for two-switch buck-boost dc-dc converter," *IEEE Trans. Power Electron.*, vol. 29, no. 4, pp. 2037–2048, Apr. 2014.

[3] G. K. Andersen and F. Blaabjerg, "Current programmed control of a single-phase two-switch buck-boost power factor correction circuit," *IEEE Trans. Power Electron.*, vol. 53, no. 1, pp. 263–271, Feb. 2006.

[4] R. Morrison and M. G. Egan, "A new modulation strategy for a buck-boost input ac/dc converter," *IEEE Trans. Power Electron.*, vol. 16, no. 1, pp. 34–45, Jan. 2001.

[5] P. C. Huang, W. Q. Wu, H. H. Ho, and K. H. Chen, "High efficiency and smooth transition buck-boost converter for extending battery life in portable devices," in *Proc. IEEE Energy Convers. Congr. Expo.*, Sep. 2009, pp. 2869–2872.

[6] Y. J. Lee, A. Khaligh, A. Chakraborty, and A. Emadi, "A compensation technique for smooth transitions in a noninverting buck-boost converter," *IEEE Trans. Power Electron.*, vol. 24, no. 4, pp. 1002–1016, Apr. 2009.

[7] X. Ren, X. Ruan, H. Qian, M. Li, and Q. Chen, "Three-mode dual frequency two-edge modulation scheme for four-switch buck-boost converter," *IEEE Trans. Power Electron.*, vol. 24, no. 2, pp. 499–509, Feb. 2009.

[8] P. C. Huang, W. Q. Wu, H. H. Ho, and K. H. Chen, "Hybrid buck–boost feedforward and reduced average inductor current techniques in fast line transient and high-efficiency buck–boost converter," *IEEE Trans. Power Electron.*, vol. 25, no. 3, pp. 719–730, Mar. 2010.

[9] J. J. Chen, P. N. Shen, and Y. S. Hwang, "A high efficiency positive buck–boost converter with mode-select circuit and feed-forward techniques," *IEEE Trans. Power Electron.*, vol. 28, no. 9, pp. 4240–4247, Sep. 2013.

[10] K. C. Wu, H. H. Wu, and C. L. Wei, "Analysis and design of mixed-mode operation for non-inverting buck-boost dc-dc converters," *IEEE Trans. Circuits Syst. II: Express Briefs*, vol. 62, no. 12, pp. 1194–1198, Dec. 2015.

[11] X. E. Hong, J. F. Wu, and C. L. Wei, "98.1%-efficiency hysteretic-current-mode noninverting buck-boost dc-dc converter with smooth mode transition," *IEEE Trans. Power Electron.*, vol. 32, no. 3, pp. 2008–2017, Mar. 2017.

[12] C. L. Wei, C. H. Chen, K. C. Wu, and I. T. Ko, "Design of an average current- mode noninverting buck–boost dc–dc converter with reduced switching and conduction losses," *IEEE Trans. Power Electron.*, vol. 27, no. 12, pp. 4934–4943, Dec. 2012.

[13] C. Restrepo, J. Calvente, A. Cid, A. El Aroudi, and R. Giral, "A noninverting buck-boost dc-dc switching converter with high efficiency and wide bandwidth," *IEEE Trans. Power Electron.*, vol. 26, no. 9, pp. 2490–2503, Sep. 2011.

[14] C. Restrepo, J. Calvente, A. Romero, E. Vidal-Idiarte, and R. Giral, "Current mode control of a coupled-inductor buck-boost dc-dc switching converter," *IEEE Trans. Power Electron.*, vol. 27, no. 5, pp. 2536–2549, May 2012.

[15] R. Paul and D. Maksimovic, "Analysis of PWM nonlinearity in non-inverting buck-boost power converters," in *Proc. 2008 IEEE Power Electron. Spec. Conf.*, 2008, pp. 3741–3747.

[16] D. C. Jones and R. W. Erickson, "A nonlinear state machine for dead zone avoidance and mitigation in a synchronous noninverting buck-boost converter," *IEEE Trans. Power Electron.*, vol. 28, no. 1, pp. 467–480, Jan. 2013.

[17] C. Restrepo, T. Konjedic, J. Clavente, and R. Giral, "Hysteric transition method for avoiding the dead-zone effect and subharmonics in a non-inverting buck–boost converter," *IEEE Trans. Power Electron.*, vol. 30, no. 6, pp. 3418–3430, Jun. 2015.

[18] Y. Ma, S. Wang, S. Zhang, and X. Fan, "An automatic peak-valley current mode step-up/step-down dc-dc converter with smooth transition," in *Proc. IEEE 10th Int. Conf. ASIC*, 2013, pp. 1–4.

[19] R. Lin and R. Wang, "Non-inverting buck-boost power-factor-correction converter with wide input-voltage-range applications," in *Proc. 36th Annu. Conf. IEEE Ind. Electron. Soc.*, Nov. 2010, pp. 599–604.

[20] Y. Y. Tsai, Y. S. Tsai, C. W. Tsai, and C. H. T. Sai, "Digital noninverting-buck-boost converter with enhanced duty-cycle-overlap control," *IEEE Trans. Circuits Syst. II: Express Briefs*, vol. 64, no. 1, pp. 41–45, Jan. 2017.

[21] D. Jones and R. Erickson, "Buck-boost converter efficiency maximization via a nonlinear digital control mapping for adaptive effective switching frequency," *IEEE J. Emerging Sel. Topics Power Electron.*, vol. 1, no. 3, pp. 153–165, Sep. 2013.

[22] D. H. Kim and B. K. Lee, "An enhanced control algorithm for improving the light-load-efficiency of noninverting synchronous buck-boost converters," *IEEE Trans. Power Electron.*, vol. 31, no. 5, pp. 3395–3399, May 2016.

Authors' photographs and biographies not available at the time of publication.